Flight Control System Design and Sizing Methodology for hypersonic cruiser

Flight Control System Design and Sizing Methodology for hypersonic cruiser

Roberta Fusaro[1], Davide Ferretto[2] and Nicole Viola[3]
Politecnico di Torino, Turin, 10129, Italy

Flight Control System is considered a key enabler for future high-speed aircraft and therefore, the anticipation of its impact onto the aircraft layout and performance is crucial. On one side, a preliminary characterization of the control surfaces is essential for a precise estimate of the aerodynamic characteristics of the vehicle throughout the mission. On the other side, traditional design approaches widely used in subsonic aircraft design and based on on-design and standalone system sizing, may lead to wrong estimates of the peak power demand. Conversely, typical supersonic and hypersonic design solutions are investigated by means of numerical simulations which guarantee higher accuracy but may not be directly applicable during the early design stages. Therefore, this paper discloses an innovative methodology (i) to anticipate the Flight Control System design of future high-speed aircraft at conceptual design stage, (ii) to properly consider the interactions with other subsystems and (iii) to properly predict the behavior of the Flight Control System throughout the entire mission. The integrated subsystems design methodology disclosed in this paper starts with the suggestion of the most promising semi-empirical models for control surfaces geometrical definition. The newly defined surfaces can be analyzed to predict their single contribution to the vehicle lift and drag coefficients. At this stage, the interaction with the propellant system is fundamental to identify the minimum surfaces deflections required to guarantee the aircraft trim. Indeed, in order to minimize the exploitation of control surfaces and thus limiting the detrimental effects onto the aerodynamic efficiency, propellant tanks can be properly shaped and integrated on board, and ad-hoc depletion sequencies can be adopted to match the desired center of gravity shift throughout the mission. Maximum required control surfaces deflections are used as inputs for the estimation of hinge moments to be counteract by the actuation system. A novel approach is here suggested to extend the formulation available in literature beyond the transonic regime. Eventually, the Flight Control System design is completed with the selection of actuators and finalization of the System architecture including power distribution lines and connections with the avionic system. The integrated design methodology has been developed in the context of the H2020 STRATOFLY Project and it has been exploited for the design and sizing of the Flight Control System of the STRATOFLY MR3 vehicle, a Mach 8 waverider concept for civil antipodal flights.

Nomenclature

c	=	mobile surface chord $[m]$
C_{M_0}	=	hinge moment coefficient at angle of attack equal to zero
C_{M_α}	=	hinge moment coefficient at angle of attack equal to α
C_{M_δ}	=	hinge moment coefficient for a deflection angle equal to δ

[1] Assistant Professor, Mechanical and Aerospace Engineering Department, Politecnico di Torino
[2] Assistant Professor, Mechanical and Aerospace Engineering Department, Politecnico di Torino
[3] Associate Professor, Mechanical and Aerospace Engineering Department, Politecnico di Torino

F_{flap}	=	flap force [N]
l_{flap}	=	flap length [m]
$M_{actuator}$	=	moment generated by the actuator [Nm]
M_{hinge}	=	hinge moment [Nm]
M	=	freestream Mach number
p_{flap}	=	pressure on flap [Pa]
p	=	pressure [Pa]
P	=	power demand to the actuator [W]
S	=	mobile surface area $[m^2]$
V	=	airspeed $\left[\frac{m}{s}\right]$
w_{flap}	=	flap width [m]
α	=	angle of attack
β_0	=	oblique shock wave angle
δ	=	deflection angle of the control surface
η	=	efficiency of the transmission
θ_0	=	wedge angle of the lower part of the vehicle
ρ	=	air density in $\left[\frac{kg}{m^3}\right]$
ω	=	angular speed of the control surface [rad/s]

CoG	Centre of Gravity
FCS	Flight Control System

I. Introduction

Flight Control System is considered a key enabler for future high-speed aircraft and therefore, the anticipation of its impact onto the aircraft layout and performance is essential to assess the viability of under-development concept. Preliminary investigations carried out in several high-speed projects [1], [2], [3],[4] highlight that a reduction of about 30% with respect to the maximum theoretical efficiency of a hypersonic civil aircraft can be expected due to control surfaces deflection. Therefore, anticipating the effect of Flight Control System (FCS) onto the vehicle behavior, since the early stage of design guarantees a more accurate and realistic aerodynamic characterization and the consequent more reliable estimation of fuel consumption and range performance. In turn, a more reliable estimate of the aircraft fuel consumption for high-speed aircraft is a key element for the estimation of the environmental impact of the vehicle and mission concept [2] [5] as well as for the economic viability of the solution [6][7].

Traditional subsystems design methodologies are not directly applicable to supersonic and hypersonic vehicles for different reasons. Hereafter, the main reasons requiring a paradigm shift in subsystem design methodology are reported, together with an indication of the main novelties introduced in this paper to overcome the highlighted limitations.

First of all, subsystems design methodologies available in literature, such as the well-known Roskam [8], Torenbeek [9], Raymer [10], and the more recent Sadraey [11] consider each subsystem as standalone and possible interactions with other subsystems are accounted for only during the detailed design phases. This simplification is acceptable for subsonic aircraft, where each main high-level functions is specifically allocated onto a well-defined subsystem. However, this is not the case for high-speed vehicles. Indeed, both supersonic and hypersonic transportation systems are characterized by a high-level of integration both from the aero-thermo-propulsive standpoint as well as from the subsystem one. The high-level of integration at subsystem level is twofold. On one side, there are clear examples of multifunctional subsystems, which integrate in a single physical equipment, more than a single high-level capability. On the other side, in order to reach the expected unprecedented performance target, it is essential to increase the integration and interactions among the various on-board subsystems. This is the case of Flight Control Subsystem, whose design and sizing shall consider the strict relationship with the propellant subsystem.

Secondly, the subsystems design methodologies available in literature indicate the cruise as sizing condition for most of the subsystems, including the Flight Control Subsystem. This assumption perfectly fits the case of subsonic aircraft, but it is not representative for supersonic and hypersonic aircraft as already demonstrated in [12]. Depending on the vehicle confirmation and mission, subsonic flight conditions (such as take-off and landing) can be more demanding for the FCS than the high-speed cruise one. Therefore, the FCS design methodology shall include rapid estimation of the actuation power required in each different mission phase, thus allowing for an adequate selection of the reference sizing condition.

Thirdly, following classical conceptual design methodologies, the impact of control surfaces deflection onto the aircraft aerodynamic characterization can be neglected during the early stage of design, without extreme penalties. This can be acceptable for subsonic aircraft with traditional wing-fuselage architecture, whilst it cannot be applied to the case of high-speed aircraft, mostly characterized by non-conventional configurations, including waverider concepts. As clearly shown in [4], the impact of control surfaces deflection can noticeably affect the aerodynamic performance of the entire vehicle. Therefore, the FCS design methodology shall be supported by a first indication of the effect of each control surfaces actuation, throughout the mission profile. This preliminary estimation paves the way for the integration of trim analysis and consequently for a more accurate mission analysis.

Lastly, Subsystems Design traditionally pertains to the Preliminary Design phase, thus it uses the results of the Conceptual design phase as input. However, this waterfall approach is hardly applicable to the design of Subsystem for highly integrated vehicle concept where each on-board subsystem has an evident impact on the vehicle and mission concept. Therefore, the conceptual design methodology suggested in this paper adopts an agile approach (opposite to the traditional waterfall concept), which encourages fast iterations involving different design levels and a level of accuracy which incrementally increases through each iteration.

In view of this context, in order to improve the accuracy of conceptual design for future supersonic and hypersonic vehicles, this paper discloses an innovative methodology able to anticipate the design and sizing of Flight Control System at conceptual design stage, to properly consider the interactions with other subsystems and to properly predict the behavior of the system throughout the entire mission. In the next sections, the integrated design approach is presented, with special focus on the element of novelties introduced with respect to the state-of-the-art approach and the application to the STRATOFLY MR3, a Mach 8 waverider for long-haul routes is reported and results

II. Integrated Design Methodology

A. Methodology overview

Fig. 1 graphically summarizes the integrated system design methodology here suggested to support the preliminary design and sizing of Flight Control System. In addition to the intrinsic novelty of the integrated design approach, Figure 1 marks with red labels the innovative contributions included in this paper.

The integrated system methodology suggests the possibility to introduce the FCS in the design loop as soon as a first aircraft external layout is available as well as its first aerodynamic and propulsive characterization. On this basis, a preliminary mission analysis can be carried to identify a viable flight trajectory and to verify the behavior of the vehicle concept throughout the mission. Indeed, for high-speed vehicle design, it is essential to check the major aerodynamic and propulsive characteristics in off-design conditions, i.e. at subsonic and low supersonic speed regimes, to ensure the feasibility of the concept. Once a first conceptual design loop is completed, it is the proper time to introduce the analysis of the Flight Control System, starting from educated guesses for the geometrical characterization of empennages and related control surfaces. Few promising semi-empirical models for control surfaces geometrical definition are available in literature and they use the volumetric ratios as many design parameters [12]. These simplified semi-empirical models are very useful to geometrically define chords and widths of each control surface and the consequent evaluation of the distance between their aerodynamic center and the one of the entire vehicle. Once all control surfaces are defined, it is essential to estimate their maximum deflections. In this case, differently from the subsonic aircraft design, where typical deflections can be suggested according to literature and long-time experience, for high-speed aircraft it is essential to estimate the minimum deflections requested to meet trim requirements throughout the mission. It is at this stage that the interaction with a second loop of conceptual design is necessary as well as the integration of inputs coming from the preliminary investigation

of propellant and avionic systems. In details, the newly defined surfaces can be analyzed with low- or high-fidelity aerodynamic tools to predict their single contribution to the vehicle lift and drag coefficients. According to [4], the effect of control surfaces deflection can be estimated through inviscid calculations applied to simplified configurations where depending on the specific integration issues of the surface with the airframe, standalone or integrated simulations can be performed. The contribution of the control surfaces is thus evaluated with respect to the clean configuration case, i.e. the results of the aerodynamic characterization of the vehicle with undeflected control surfaces as carried out during the first loop of conceptual design. The upgraded aerodynamic characterization can be exploited for a second mission analysis where the vehicle trim conditions are estimated for each single point of the mission. However, at this point, the interaction with the propellant system design and avionics becomes crucial. Indeed, trim conditions strongly depend on the position of the aircraft center of gravity, whose variation along a long-haul route hypersonic mission cannot be neglected. Therefore, prior to the definition of real control surfaces deflections it is essential to study and implement a proper tank distribution and depletion strategy to minimize control surface deflections and thus reducing the detrimental effect on the overall aircraft aerodynamic efficiency. It is also important to notice that for high-speed aircraft, in line with the approach adopted for military aircraft, a reduction in stability can be accepted, especially in low supersonic flight regime, to reduce trim drag penalty. In case a reduced stability approach is pursued, it is essential to immediately inform the avionics design team to ensure that artificial augmented stability functionalities are included into the system architecture. Finally, maximum required control surfaces deflections are used as inputs for the estimation of hinge moments to be counteracted by the actuation system. A novel approach is suggested in the following subsection, to extend the formulations available in literature [14], beyond the transonic regime. Eventually, the Flight Control System design is completed with the selection of actuators and finalization of the System architecture including power distribution lines and connections with the avionic system and the electrical power system.

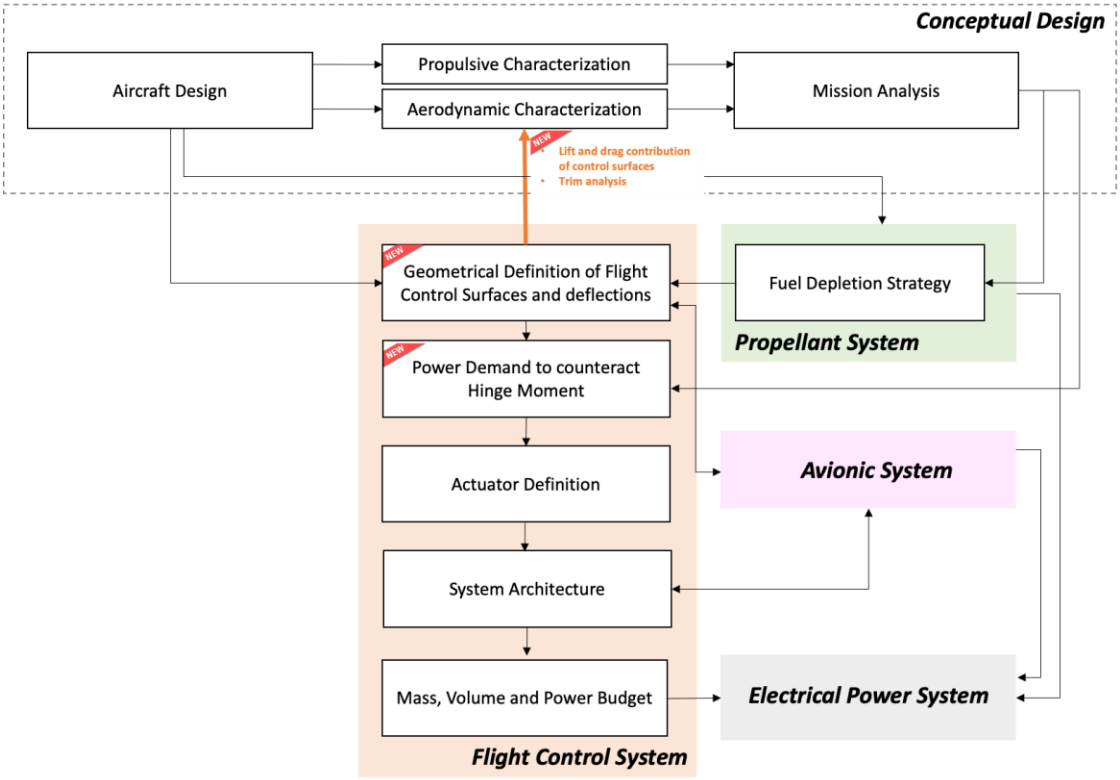

Fig. 1: Integrated FCS Design Methodology

Hereafter, a detailed description of the algorithm for the estimation of power demand to counteract the hinge moment throughout the entire mission profile is provided.

B. Detailed Estimation of Power Demand to Counteract Hinge Moment

Figure 2 summarizes the algorithm for the estimation of power demand to counteract the hinge moment throughout the entire mission. The reference trajectory can be discretised, and one or more points are selected and evaluated per each flight segment. Specifically, if the flight condition under investigation is characterized by a Mach number lower than 2, traditional approaches can be exploited [14]. In this case the hinge moment is evaluated as function of the hinge moment coefficient which in turns depends on the aircraft angle of attack and the maximum deflection foreseen in that specific condition.

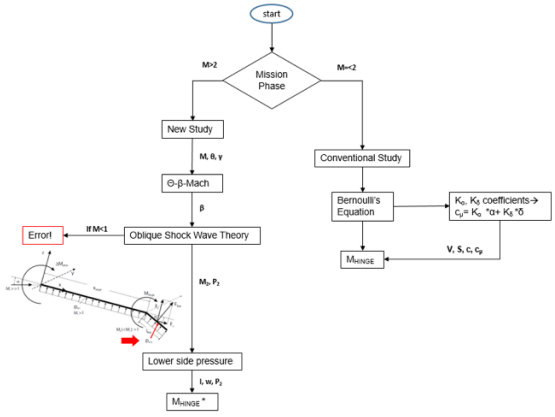

Fig. 2: Hinge Moment estimation algorithm

Therefore up to Mach 2, considering the mission profile and given the coefficients $C_{M_0}, C_{M_\alpha}, C_{M_\delta}$, the deflection δ of the mobile surface and the angle of attack, α, the hinge moment is obtained as in (1).

$$M_{hinge} = \frac{1}{2}\rho V^2 S c C_M \qquad (1)$$

Where ρ is the air density in $\left[\frac{kg}{m^3}\right]$, V is the airspeed $\left[\frac{m}{s}\right]$, S is the mobile surface area $[m^2]$, c is the mobile surface chord $[m]$.

$$C_M = C_{M_0} + C_{M_\alpha}\alpha + C_{M_\delta}\delta \quad (2)$$

Conversely, for flight speed higher than Mach 2 the theory illustrated above is not acceptable. An algorithm based on the oblique-shock theory is here suggested to overcome this limitation. In details, to determine the hinge moment of the control surface exposed to a supersonic flow, it is necessary to study the oblique shock waves formation from the aircraft leading edge up to the area of the movable surface itself. Figure 3 shows an idealized flight vehicle with a deflected control surface as reported in [12]

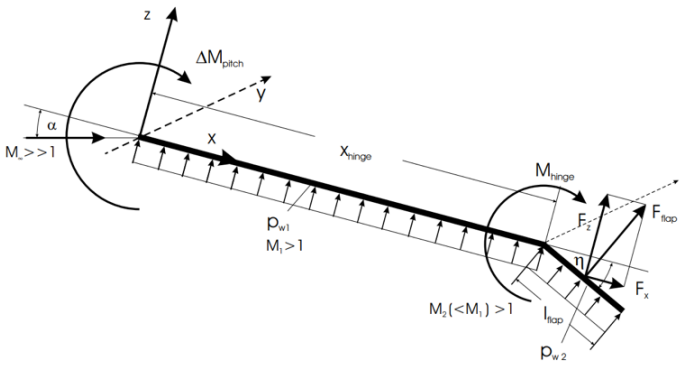

Fig. 3: Ideal vehicle representation

Here it is assumed that a constant pressure p_{w_1} acts on the lower side of the vehicle, whereas a constant $p_{w_2} = p_{flap}$ acts on the lower side of the deflected control surface (this is the ideal inviscid case) [6] which has the dimensions (length) l_{flap} and (width) w_{flap}. The flap force F_{flap} is then computed as in Eq. (3).

$$\mathbf{F_{flap} = l_{flap} w_{flap} p_{flap}} \quad (3)$$

The flap force times its lever arm with respect to the flap axis must be balanced by the hinge moment, as reported in Eq. (4).

$$\mathbf{M_{actuator} = -M_{hinge} = -\frac{l_{flap}}{2} F_{flap} = -\frac{l_{flap}^2}{2} w_{flap} p_{flap}} \quad (4)$$

The theory of oblique shock wave is used to determine pressure value acting on the lower side of the vehicle. For complex hypersonic configurations, such as the one reported in Fig. 4, the external flow can face multiple shocks before reaching the leading edge of the control surface.

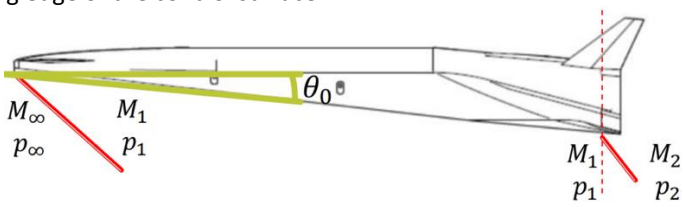

Fig. 4: Schematical representation of Oblique shock formations along a waverider configuration

Through the $\theta - \beta - Mach$ relationship reported in Eq. (5), it is possible to find out the shock angle β produced by the θ deflection at that Mach number.

$$\mathbf{\tan \theta_0 = 2 \cot g \, \beta_0 \frac{(M_\infty \sin \beta_0)^2 - 1}{M_\infty^2 (\gamma + \cos 2\beta_0) + 2}} \quad (5)$$

Once the oblique shock wave angle β_0 is defined, it is possible to estimate the characteristics of the flow after the oblique shock. Knowing the characteristics of the flow in front of the oblique shock, in particular the Mach number, $M_0 = M_\infty$, and the static pressure, $p_0 = p_\infty$, it is possible to estimate the static pressure, p_1, and the Mach number, M_1, behind the shock as in Eq. (6) and Eq. (7).

$$p_1 = p_0 \left(1 + \frac{2\gamma(M_0^2 \sin^2 \beta_0 - 1)}{1 + \gamma}\right) \quad (6)$$

$$M1 = \frac{1}{\sin(\beta_0 - \theta_0)} \sqrt{\frac{(\gamma - 1)(M_0 \sin \beta_0)^2 + 2}{2\gamma(M_0 \sin \beta_0)^2 - (\gamma - 1)}} \quad (7)$$

Then it is possible to evaluate the pressure acting on the deflected control surface. Through the $\theta - \beta - Mach$ relationship, it is possible to find out the shock angle β_1 produced by the θ_1 deflection of the control surface at Mach

number M_1 evaluated in the first step. Then the estimation of the characteristics of the flow, after the second oblique shock wave, are determined (8).

$$p_2 = p_1\left(1 + \frac{2\gamma(M_1^2 \sin^2 \beta_1 - 1)}{1+\gamma}\right) \quad (8)$$

Once the values of the hinge moments are known, the required power can be estimated as in Eq. (9), assuming the hydraulic analogy for actuation devices.

$$P = \frac{2}{3} \cdot M_{hinge} \cdot \frac{\omega}{\sqrt{3}} \cdot \frac{1}{\eta} \quad (9)$$

Where M_{hinge} is the hinge moment previously determined in [Nm], ω is the angular speed of the surface [rad/s] and η is the efficiency of the transmission.

III. STRATOFLY MR3 case study

A. STRATOFLY MR3 vehicle and mission concepts

STRATOFLY MR3 is a highly integrated vehicle, where propulsion, aerothermodynamics, structures and on-board subsystems are strictly interrelated to one another, as highlighted in Fig. 5. Looking inside the aircraft, the use of a bubble structure has successfully demonstrated to achieve lightweight airframe with multi-functional roles, such as passenger cabin, multiple split tanks with anti-slosh baffles, engine bays, intake flow-paths etc., to eventually integrate all subsystems in a harmonious way. Liquid hydrogen has been selected as propellant, thanks to its high specific energy content. The high specific energy of the liquid hydrogen allows the vehicle to cover antipodal routes flying at Mach 8, without emitting any CO_2. In the first part of the project, conceptual design methods and tools have been used to preliminary assess mass, volume and power budgets following a top-down approach. Subsequently, in the second part of the project, those analysis have been verified through the design, sizing, integration and in some cases simulation of each subsystem.

The STRATOFLY MR3 vehicle has been originally conceived to cover antipodal routes with a distance flown up to 19000 km. During the first part of the mission the ATR engines are used. The vehicle flies at subsonic speeds during the first phase, which is called subsonic climb. The vehicle accelerates from Mach=0.37 to Mach=0.95 at an altitude between 11 km and 13 km. Then, the vehicle performs the subsonic cruise. This phase is needed to avoid the sonic boom while flying over land. A constraint on the distance flown from the departure site is introduced to fulfil this requirement: the subsonic cruise phase ends when the vehicle is at 400 km from the departure airport. During the next phase, the vehicle performs a second climb, until it reaches the Mach number of 4 (supersonic climb). At the end of this phase, the ATR engines are turned off and the DMR is activated to accelerate up to Mach=8 at an altitude of 32-33 km (hypersonic climb). Here, the cruise starts at a constant Mach number of 8 and at an altitude between 32 and 36 km. During the first part of the cruise, the vehicle flies over the arctic region towards the Bering strait, between Asia and North America. Then, the vehicle continues to cruise over the Pacific Ocean towards Sydney. The cruise phase is over when a certain distance from the landing site is reached. This distance depends on the type of descent considered, i.e. propelled or gliding descent. The first mission concept involved a gliding descent. However, since the aerodynamic performance are very low in engine-off conditions, a propelled descent has been considered for the final version of the mission concept. The results of the reference trajectory simulation are reported in the following figures. The Brussels to Sydney mission can be completed with a total travel time of 3hr 24min. An overview of the complete trajectory is reported in [2], where the main characteristics of the trajectory can be clearly identified. The vehicle performs its cruise over the polar region, flying towards the Bering strait. Then it passes over the Pacific Ocean, while flying towards the destination airport.

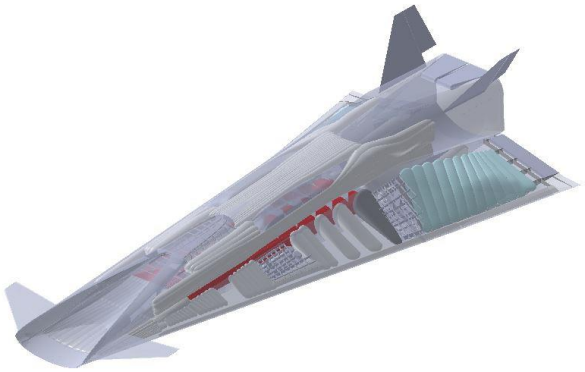

Fig. 5: STRATOFLY MR3 Vehicle layout with integrated subsystem

The altitude and Mach profile of the STRATOFLY MR3 vehicle are reported in Fig. 6. The time required to perform the subsonic climb and cruise phases is equal to 26 min, while the time required to perform the supersonic and hypersonic climb is equal to 29 min. A total time of 55 min is needed to reach the begin of cruise conditions, while the cruise phase lasts 1h 29min.

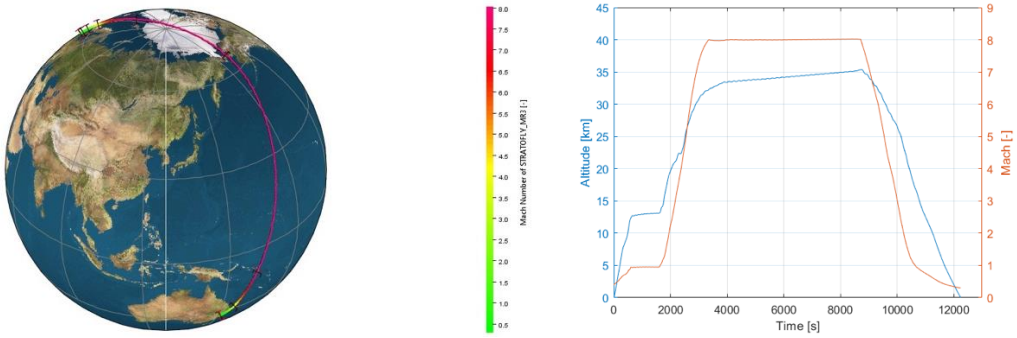

Fig. 6: Overview of complete trajectory BRU-SYD.

The profile of the Mach number versus Distance flown is reported in Fig.6. The propellant mass variation over time is shown in Fig. 7. As expected, the highest consumption rate is experienced at the beginning of the mission, while the vehicle performs the climb phases. During cruise instead the propellant mass consumption is reduced. A total of 179 t of propellant mass is needed to complete the mission, while about 2 t are left at the end.

The lift to drag ratio profile is also reported in Fig.7. The L/D is maximised during cruise and it is equal to 7, while its lowest value (L/D≈3) is found during the supersonic climb. Moreover, the same Figure also reports the angle of attack used during the mission. Value of AoA lower than zero are needed throughout the entire mission. If the AoA is different from zero, the vehicle flies in non-optimal condition from the point of view of the aerodynamic and propulsive performance. However, the use of low AoAs is required to avoid that the vehicle generates too much lift due to its large lifting surface, which would result in a fast gain/loss of altitude and in an increase of the Rate of Climb/Descend.

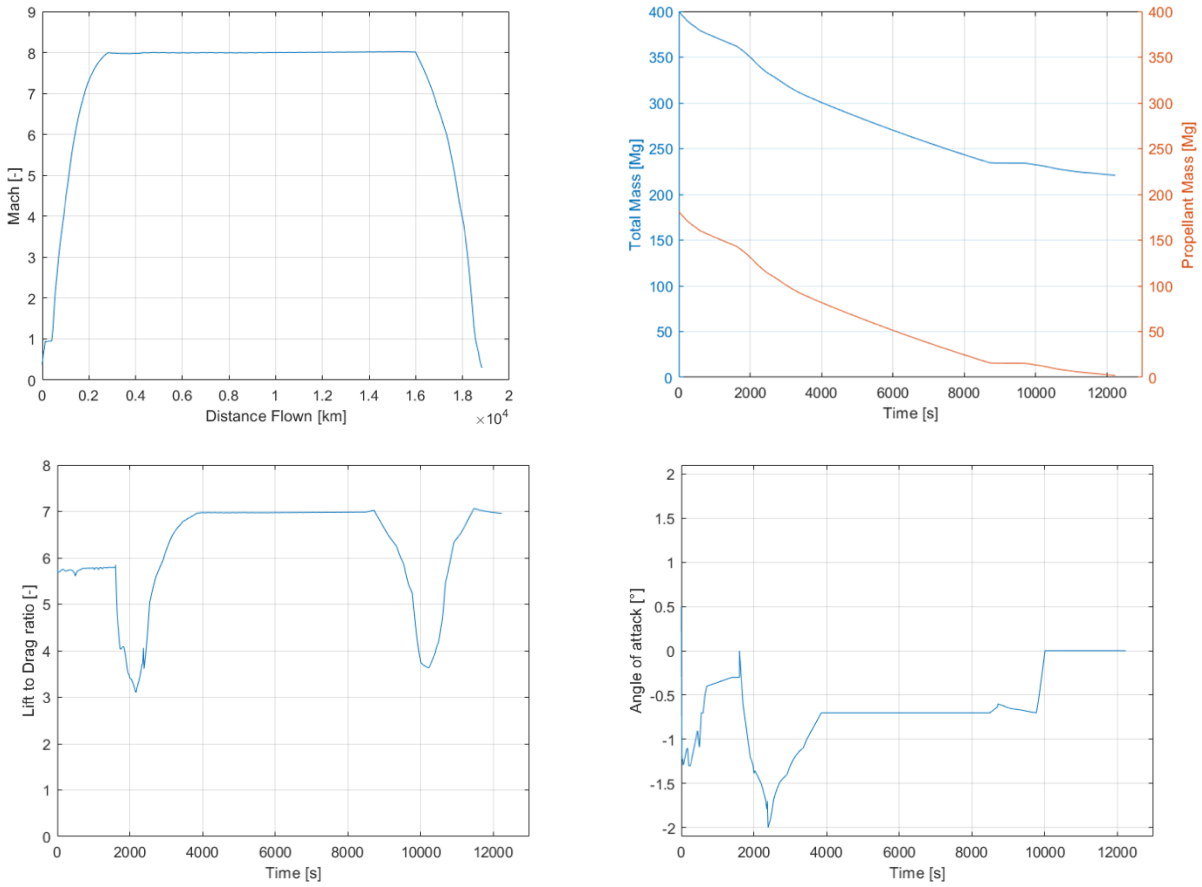

Fig. 7: Main results of the Mission Analysis of STRATOFLY MR3.

B. Control surfaces Design & Integration

Fig. 8 summarizes the results of the Geometrical Definition of all control surfaces integrated in STRATOFLY MR3 configuration. Specifically, the final aircraft layout includes a fully movable canard, 4 elevons, 2 body flaps placed on top of the integrated nozzle and a pair of V-shaped rudders.

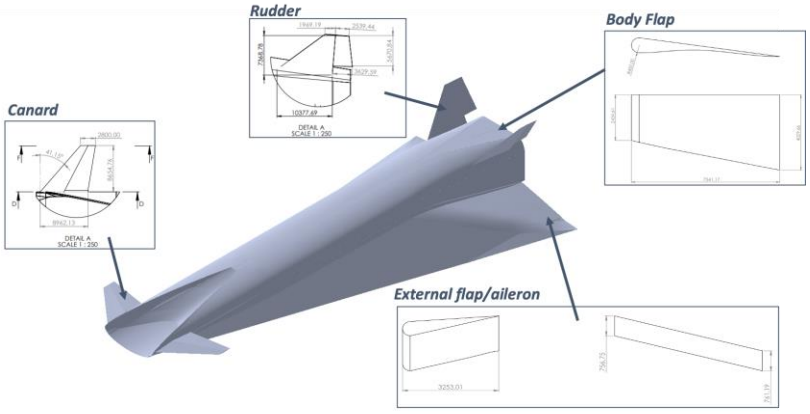

External Elevon (single surface)	
Chord [m]	3
Span [m]	5
Maximum deflection [°]	+/- 25
Surface [m^2]	15
Internal Elevon (single surface)	
Chord [m]	3
Span [m]	5
Maximum deflection [°]	+/- 25
Surface [m^2]	15
Canard (single surface)	
Root chord [m]	8.7
Tip chord [m]	2.8
Span [m]	8.7
Maximum deflection [°]	+/- 20
Sweep angle [°]	49
Surface [m^2]	50
Rudder (single surface)	
Major chord [m]	3.6
Tip chord [m]	2.5
Height [m]	6.5
Maximum deflection [°]	+/- 20
Inclination [°]	33
Surface [m^2]	19.8
Body flap (single surface)	
Root span [m]	4.05
Tip span [m]	2.58
Length [m]	7.14
Maximum deflection [°]	+ 30
Surface [m^2]	23.7

Fig. 8: STRATOFLY MR3 Control Surfaces Geometrical Definition

C. Aerodynamic Characterization and Trim analysis

The control surfaces described in Fig. 8 have been thoroughly investigated from the aerodynamic standpoint to estimate their impact onto the overall aircraft aerodynamic efficiency. Details of the aerodynamic computations have been published in [4]. Once all the aerodynamic computations have been completed, the trim analysis has been performed. Among the full set of stable conditions evaluated during the previous step, it is possible to select the surfaces deflections and the corresponding angle of attack α_{trim} which guarantee $C_{My}=0$. The first output of this analysis is a set of trim maps, as the ones reported in Fig. 9. The 3D map shows the resulting α_{trim}, that corresponds to the trimmed state, as a function of bodyflap and flap deflections, for Mach=8 and CoG=48 m. Each canard deflection δ_{canard} is reported with a different color. Fig. 9b also shows similar results. However, in this plot the bodyflap deflection is fixed and the angle of attack α_{trim} varies only with the flap deflection δ_{flap}.

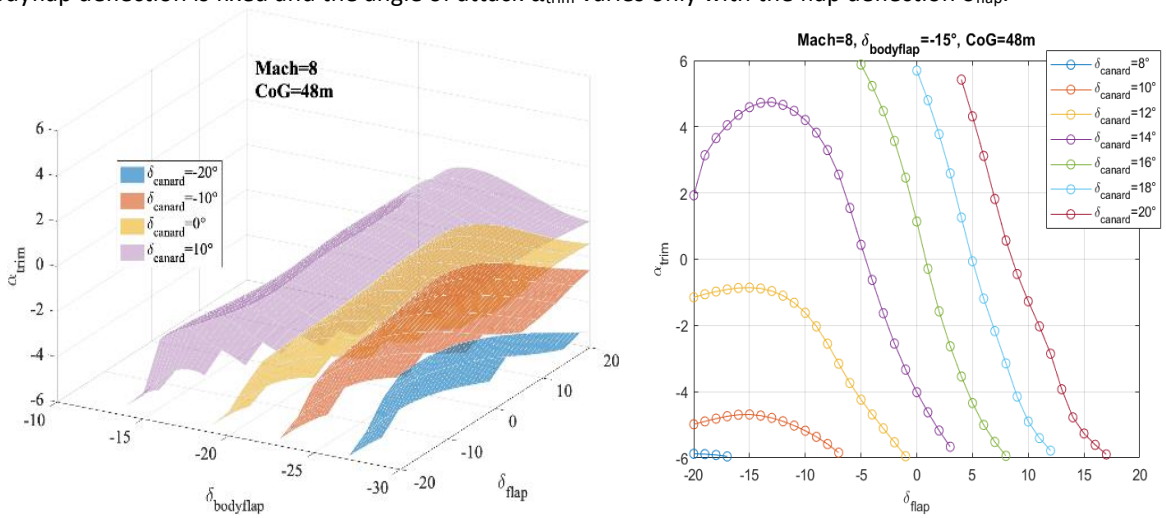

Fig. 9: STRATOFLY MR3 3D and 2D trim maps examples

Since the STRATOFLY MR3 vehicle is supposed to fly at low angles of attack, only α_{trim} between -2° and 2° are considered for the analysis. For each α_{trim}, the corresponding C_L and C_D can be also evaluated and, accordingly, the L/D. Moreover, for a given Mach number and CoG position, the same α_{trim} can be achieved with different combinations of control surfaces deflections. However, only one combination should be selected to be used as an input for the mission simulation in ASTOS. The combination that corresponds to the highest L/D is selected, to maximize the aerodynamic performance. Eventually, the complete trimmed aerodynamic database can be derived and used as an input to perform the mission simulation. The resulting C_L, C_D and L/D, at different Mach numbers and for AoA=0°, are reported in Fig. 10 and Fig. 11. The impact of the deflections of the control surfaces is clearly visible, especially for what concerns the increase in total drag and, consequently, the decrease of the aerodynamic efficiency along the entire Mach range. The lowest value of the Lift to Drag ratio is found at supersonic speed, in the range from Mach 0.9 to 3, where the L/D decrease to 3.5-4. From a preliminary mission simulation, it has been found that the time required to perform the supersonic climb (i.e. accelerating from Mach 0.95 to Mach 4) can be quite high and could limit the capability of the STRATOFLY vehicle to cover the antipodal route. For that reason, a possible solution can be to relax the stability requirements within this range, taking advantage from the modern, robust and fast GNC equipment. Therefore, the constraint on longitudinal static stability is removed and the trim conditions are evaluated again in this range, considering that $\delta C_{My}/\delta\alpha > 0$. The resulting L/D is reported in Fig. 11, where the continuous line represents the trim conditions with static stability and the dashed line refers to the unstable case. The aerodynamic efficiency is slightly increasing in this range, even if the increase is limited to values below 0.5.

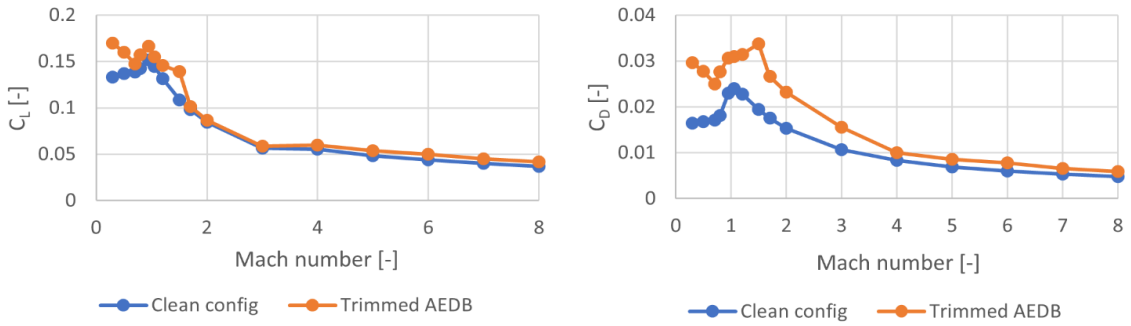

Fig. 10: Comparison of the C_L and C_D between clean configuration and trimmed case, for different Mach numbers

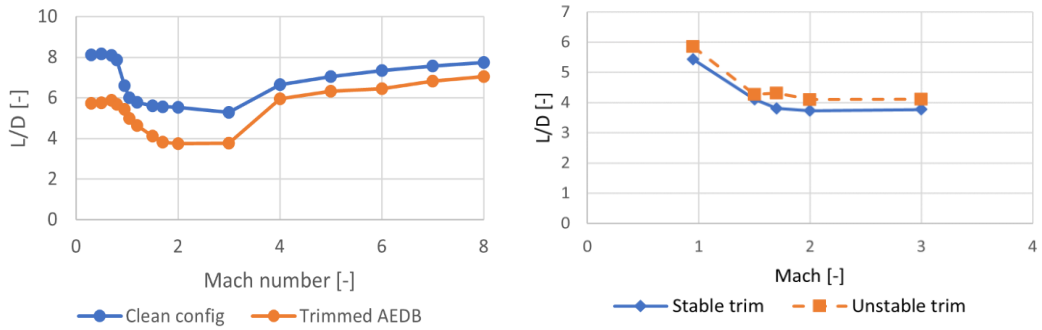

Fig. 11: Comparison of the L/D between clean configuration and trimmed case, for different Mach numbers and Comparison between the Lift to Drag ratio of the stable and unstable conditions at supersonic Mach

The optimized propellant depletion strategy and its effect onto the body-flap deflection is reported in Fig. 12 as example, together with a summary of all surfaces deflections throughout the entire reference trajectory.

		CoG position - Climb/Cruise										
		53	52.5	52	51.5	51	50.5	50	49.5	49	48.5	48
Mach	0.3	-30	-25	-25	-25	-25	-25	-20	-20	-20	-10	0
	0.5	-30	-25	-25	-25	-25	-20	-20	-20	-10	0	0
	0.7	-25	-25	-25	-20	-20	-20	-10	0	0	0	0
	0.8	-25	-25	-25	-20	-20	0	0	0	0	0	0
	0.95	-20	-20	-20	-15	0	0	0	0	0	0	0
	1.05	-25	-20	-20	0	0	0	0	0	0	0	0
	1.2	-25	-20	-20	0	0	0	0	0	0	0	0
	1.5	-25	-25	-20	-20	-20	0	0	0	0	-10	-10
	1.7	-25	-25	-25	-20	-20	-20	-15	-10	-10	-10	-10
	2	-25	-25	-25	-20	-20	-20	-20	-15	-10	-10	-10
	3	-25	-25	-25	-25	-25	-25	-20	-20	-20	-20	-15
	4	-25	-25	-25	-20	-20	-20	-15	-15	-10	0	0
	5	-25	-25	-25	-20	-20	-20	-15	0	0	0	0
	6	-25	-25	-20	-20	-20	-20	-15	-15	0	0	0
	7	-25	-25	-20	-20	-20	-20	-15	0	0	0	0
	8	-25	-25	-20	-20	-20	-20	-15	-15	-15	-10	0

Fig. 12: Effect of the optimized propellant depletion profile (in terms of CoG displacement) onto the body-flap deflection and a summary of all surfaces deflections throughout the entire reference trajectory

D. Actuation System Sizing

As a result of the application of the twofold algorithm for hinge moment estimation, power demand per each control surface has been obtained and it is available in Fig. 13 together with the overall FCS power demand. It clearly emerges that the most critical phases from the point of view of the required power are those at take-off, low supersonic acceleration and approach, where peaks of over 130kW are reached, while an average 20kW are sufficient to support deflections in hypersonic cruise. From an operational point of view, the surface that requires highest power level is the body flap, with a peak of about 45 kW.

It is therefore important to notice that in this case, considering cruise condition as reference sizing condition would have caused a dramatic error.

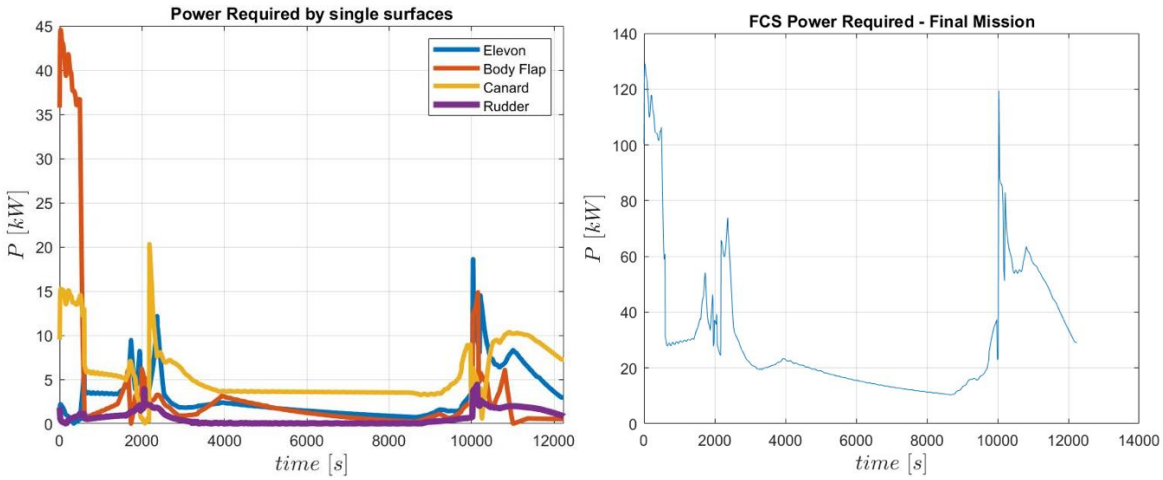

Fig. 13: power demand per each control surface and final FCS power budget.

According to what is illustrated in the methodology section, peak values can be directly associated to actuation mass, as reported in Table 1.

Table 1. Actuators mass

	Single Surface Actuator Mass [kg]
Elevon	74.4
Body Flap	178.3
Canard	81.2
Rudder	17.7

Better performance can be expected also considering technology improvement and far-term Entry-Into-Service (EIS) of the vehicle. Technological progress can lead to a reduction of about 30% in terms of weight compared to the values of equipments currently available on the market. This affects not only costs but also the inertia of the entire system.
At the actual state of the art, the overall mass of actuators is estimated around 852 kg.

E. Flight Control System Architecture

For the STRATOFLY MR3 aircraft, given the reduced amount of movable surfaces to be controlled (with reference to conventional airliners), the Boeing-type solution was selected, where three Primary Flight Computers (PFCs) each of which has three similar lines with dissimilar hardware but the same software. Each line has a separate role during an operating period and the roles are cycled after power up. The Actuator Control Electronics (ACE) units directly drive the flight control actuators.

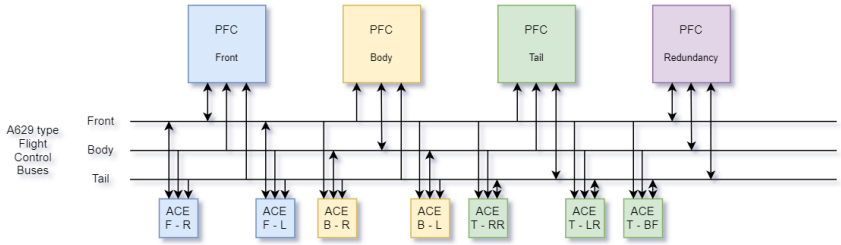

Fig. 14: Proposal for FCS actuators control architecture on STRATOFLY MR3

The system is made up of four Primary Flight Computers (PFCs), three of which are always operative: the Front, tho Body and the Tailand one is in redundancy. They consist of three different inner sections, each one with a very specific task:

- Command: it processes and supplies the output commands;
- Standby: performs the same processes of Command and returns output only when the Command is no longer operational (failure);
- Monitor: performs the same calculations as the previous ones and uses them to verify their consistency by intervening in the event of failure.

The redundant computer is also made up of three sections, however they are all in "Command" mode. This ensures that it can completely replace a possible failure in the command line of one of the main computers. If necessary, it is able to completely replace the command lines of each of the 3 main PFCs, allowing the mission to be completed successfully. Each single PFC interfaces with 7 Actuator Control Electronics (ACE) divided as follows (Fig. 15):

- Two for the elevons, one on the right and one on the left: 2 x ACE body;
- One for the body flaps and two for the rudders: 3 x ACE tail;
- Two for the Canard, one on the right and one on the left: 2 x ACE front.

Fig. 16 instead reports a proposal for what concerns electrical feeding of the main actuation elements on the STRATOFLY MR3 FCS. On each side of the Canard there are 3 actuators, two of which are always operational and one in redundancy. Each elevon, is moved by two actuators, one always operational and one in redundancy. In turn, each body flap is moved by two actuators, one of which is operational and one in redundancy. The same applies to the rudder.Three electrical distribution lines grant fail-safe architecture. They consist of three independent electrical circuits: yellow, blue and red. Yellow and blue circuits are connected with actuators that move the mobile surface for each mission phase. The red line is responsible for supplying the actuators in redundancy and is activated only in the event of failure of one of the main lines. The approach used was to adopt two different lines for symmetrical moving surfaces with respect to the x - axis of the aircraft. In this way, the failure on one line is prevented from damaging the entire operation of that specific mobile surface.

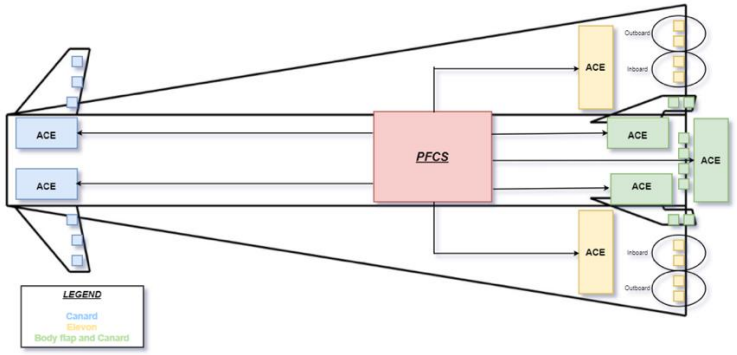

Fig. 15: Possible actuators control architecture

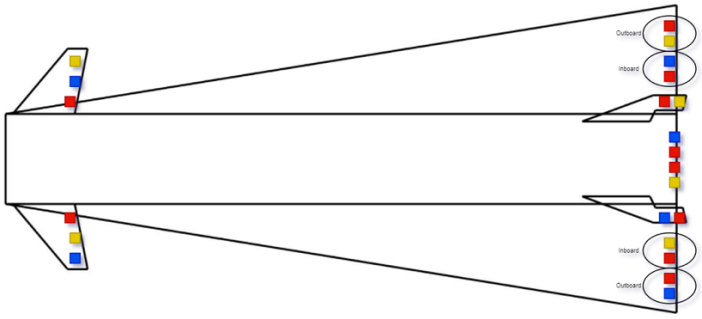

Fig. 16: Possible actuators power distribution architecture

IV. Conclusion

This paper discloses an innovative methodology which pursues three main objectives: (i) to anticipate the Flight Control System design of future high-speed aircraft at conceptual design stage, (ii) to properly consider the interactions with other subsystems and (iii) to properly predict the behavior of the Flight Control System throughout the entire mission. The integrated subsystems design methodology disclosed in this paper starts with the suggestion of the most promising semi-empirical models for control surfaces geometrical definition. The newly defined surfaces can be analyzed to predict their single contribution to the vehicle lift and drag coefficients. At this stage, the interaction with the propellant system is fundamental to identify the minimum surfaces deflections required to guarantee the aircraft trim. Indeed, in order to minimize the exploitation of control surfaces and thus limiting the detrimental effects onto the aerodynamic efficiency, propellant tanks can be properly shaped and integrated on board, and ad-hoc depletion sequencies can be adopted to match the desired center of gravity shift throughout the mission. Maximum required control surfaces deflections are used as inputs for the estimation of hinge moments to be counteract by the actuation system. A novel approach is here suggested to extend the formulation available in literature beyond the transonic regime. Eventually, the Flight Control System design is completed with the selection of actuators and finalization of the System architecture including power distribution lines and connections with the avionic system.

The exploitation of the methodology for the design and sizing of the Flight Control System of the STRATOFLY MR3 vehicle, a Mach 8 waverider concept for civil antipodal flights, has been very positive and it has clearly highlighted the differences with respect to traditional design methodologies.

Acknowledgments

This work has been carried out within the frame of “STRATOspheric FLYing opportunities for high-speed propulsion concepts” (STRATOFLY) project. This project has received funding from the European Union’s Horizon 2020 research and innovation program under grant agreement No 769246.

References

[1] Andro, Jean-Yves, Waldemar Rotärmel, Francesco Nebula, Gianfranco Morani, and Johan Steelant. "Design of the Actuation System for the Hexafly-Int Hypersonic Glider." Proceedings of HiSST (2018).

[2] Viola, N., Fusaro, R., Gori, O., Marini, M., Roncioni, P., Saccone, G., Saracoglu, B., Ispir, A.C., Fureby, C., Nilsson, T., Ibron, C., Zettervall, N., Bates, K.N., Vincent, A., Martinez-Schram, J., Grewe, V., Pletzer, J., Hauglustaine, D., Linke, F., Bodmer, D. Stratofly mr3 – how to reduce the environmental impact of high-speed transportation (2021) AIAA Scitech 2021 Forum, pp. 1-21. https://www.scopus.com/inward/record.uri?eid=2-s2.0-85099847756&partnerID=40&md5=cdd49e68917eff9b4e5e9a18e7660bfd

[3] Rufolo, G.C., Roncioni, P., Marini, M., Votta, R., Palazzo, S. Experimental and numerical aerodynamic data integration and aerodatabase development for the PRORA-USV-FTB_1 reusable vehicle (2006) A Collection of Technical Papers - 14th AIAA/AHI International Space Planes and Hypersonic Systems and Technologies Conference, 2, pp. 1173-1212.

[4] Viola, N., Roncioni, P., Gori, O., Fusaro, R. Aerodynamic characterization of hypersonic transportation systems and its impact on mission analysis (2021) Energies, 14 (12), art. no. 3580, DOI: 10.3390/en14123580

[5] Fusaro, Roberta, Nicole Viola, and Diego Galassini. 2021. "Sustainable Supersonic Fuel Flow Method: An Evolution of the Boeing Fuel Flow Method for Supersonic Aircraft Using Sustainable Aviation Fuels" Aerospace 8, no. 11: 331. https://doi.org/10.3390/aerospace8110331

[6] Fusaro, R., Viola, N., Ferretto, D., Vercella, V., Fernandez Villace, V., Steelant, J. Life cycle cost estimation for high-speed transportation systems (2020) CEAS Space Journal, 12 (2), pp. 213-233. DOI: 10.1007/s12567-019-00291-7

[7] Fusaro, R., Vercella, V., Ferretto, D., Viola, N., Steelant, J. Economic and environmental sustainability of liquid hydrogen fuel for hypersonic transportation systems (2020) CEAS Space Journal, 12 (3), pp. 441-462. DOI: 10.1007/s12567-020-00311-x

[8] Roskam, Jan. Airplane design. DARcorporation, 1985.
[9] Torenbeek, Egbert. Synthesis of subsonic airplane design: an introduction to the preliminary design of subsonic general aviation and transport aircraft, with emphasis on layout, aerodynamic design, propulsion and performance. Springer Science & Business Media, 2013.
[10] Raymer, Daniel. Aircraft design: a conceptual approach. American Institute of Aeronautics and Astronautics, Inc., 2012.
[11] Sadraey, Mohammad H. Aircraft design: A systems engineering approach. John Wiley & Sons, 2012.
[12] Ferretto, D., Fusaro, R., Viola, N. Innovative Multiple Matching Charts approach to support the conceptual design of hypersonic vehicles (2020) Proceedings of the Institution of Mechanical Engineers, Part G: Journal of Aerospace Engineering, 234 (12), pp. 1893-1912. DOI: 10.1177/0954410020920037
[13] Hirschel, Ernst Heinrich, and Claus Weiland. Selected aerothermodynamic design problems of hypersonic flight vehicles. Vol. 229. Springer Science & Business Media, 2009.
[14] Roskam, Jan. Airplane design. DARcorporation, 1985.